Chirality and Rotation of Asymmetric Surface-Bound Thioethers†

ARTICLE *in* THE JOURNAL OF PHYSICAL CHEMISTRY C · MAY 2010

Impact Factor: 4.77 · DOI: 10.1021/jp1026702

Chirality and Rotation of Asymmetric Surface-Bound Thioethers†

Heather L. Tierney,‡ Jeong Woo Han,§ April D. Jewell,‡ Erin V. Iski,‡ Ashleigh E. Baber,‡ David S. Sholl,§ and E. Charles H. Sykes*,‡

Department of Chemistry, Tufts University, Medford Massachusetts 02155, and School of Chemical and Biomolecular Engineering, Georgia Institute of Technology, Atlanta Georgia 30332

Received: March 24, 2010; Revised Manuscript Received: May 4, 2010

A combination of theory and experiment is used to interrogate the surface bonding geometry and rotational dynamics of a simple asymmetric thioether, butyl methyl sulfide. Calculations predict that binding occurs to a Au surface through one of the lone pairs on the sulfur atom and that the alkyl tails lie almost parallel to the surface. The unbonded lone pair remains unperturbed, and the geometry around the S atom is essentially tetrahedral, and hence two surface-bound enantiomers of the prochiral molecule are formed with an R−S inversion barrier that is predicted to be large. The rapidly rotating molecules can be clearly distinguished upon atomic-scale imaging by their mirror image pinwheel appearance. The binding of asymmetric dialkyl sulfides leads to the formation of surface-bound enantiomers, which has important consequences for studies in which thioether linkers are used in conjunction with chiral moieties and indicates that diastereomeric effects may be at play in these systems.

1. Introduction

While dialkyl sulfides have received much less attention than alkane thiols,[1–6] they have nevertheless found multiple uses in applications ranging from materials and nanoparticle synthesis to self-assembly and surface modification. The dialkyl sulfide (aka thioether) functionality has been utilized as a mediator for nanoparticle growth,[7] a linker for nanoparticle assembly,[7,8] a ligand for novel inorganic complexes,[9] and a way to tether a variety of functionalities to surfaces.[10,11] Recently, thioether linkers have proven to be effective in promoting enantioselectivity in heterogeneous catalysis by anchoring chiral modifiers to nanoparticles,[12] and asymmetric thioether intermediates have shown high enantioselectivity.[13] Little is known, however, about how the thioether functionality binds to surfaces.[14] Controversies over alkane thiol−metal interface structures[15–17] exemplify the value of a detailed atomic-level understanding of similar molecule−surface interactions. Asymmetric dialkyl sulfides have two prochiral lone pairs on the central sulfur atom and therefore may be expected to exhibit surface-bound chirality.[18–23] The earliest picture of a dialkyl sulfide−surface interaction predicted an upright geometry.[24] Despite the fact that the arrangement of the two alkyl groups and lone pairs around the central S atom on dialkyl sulfides is tetrahedral, it appears that the chirality of surface-bound asymmetric alkyl sulfides has not previously been discussed.

Surface properties of symmetric dialkyl sulfides have been investigated previously by this group and others.[10,24–32] Self-assembled monolayers (SAMs) of thioethers have been studied and compared with thiol-based SAMs.[10,24–27] Small thioethers have also been shown to act as single molecule rotors and provide an excellent test bed for studying many aspects of molecular rotation. The rotational properties of symmetric dialkyl sulfides have been studied as a function of chain length, temperature, applied voltage and tunneling current, and proximity to neighboring molecules.[28–32]

This article describes a combination of density functional theory (DFT) and scanning tunneling microscopy (STM) to investigate the adsorption of an asymmetric dialkyl sulfide, butyl methyl sulfide, on a Au(111) surface. The chiral nature of the equilibrated adsorbed molecular species was apparent in STM imaging and was further verified by optimizing its geometry and calculating its inversion barrier using DFT. Rotational properties of both enantiomers of surface-bound butyl methyl sulfide were investigated, including rotational barriers and induction of rotation using heat or tunneling current. This study reveals that upon adsorption on a Au surface, asymmetric dialkyl sulfides form two surface-bound enantiomers. The predicted inversion barrier between these two enantiomers is fairly high, so the chirality of the Au−sulfide complex may be relevant for studies involving asymmetric thioether linkers and asymmetric syntheses using these sulfide species.

2. Materials and Methods

2.1. Experimental Methods. All STM experiments were performed in a low-temperature, ultrahigh vacuum (LT-UHV) microscope built by Omicron Nanotechnology. The Au(111) sample was purchased from MaTecK and was prepared by cycles of Ar sputtering (1.0 keV/14 A) for 30 min, followed by 2 min anneal periods up to 1000 K. Approximately 12 of these sputter/anneal cycles were performed upon receiving the crystal, followed by a further 2 sputter/anneal cycles between each STM experiment. After the final anneal, the crystal was transferred in <5 min in vacuum (<5×10^{-10} mbar) to the precooled STM. In ∼30 min, the sample cooled from room temperature to either 78 or 5−7 K. All images were recorded with etched W or cut Pt/Ir tips, and voltages refer to the sample bias. Butyl methyl sulfide was obtained from the rare chemical library of Sigma Aldrich and was further purified by cycles of freeze/pump/thaw prior to introduction to the STM chamber via a leak valve. Purity was verified with mass spectra. (See the Supporting Information.) Butyl methyl sulfide was deposited onto the sample by a

† Part of the "Alfons Baiker Festschrift".
* Corresponding author.
‡ Tufts University.
§ Georgia Institute of Technology.

10.1021/jp1026702
Published on Web 05/20/2010

collimated molecular doser while the tip was scanning. The STM stage was equipped with a sample heater capable of controllably heating the sample and tip up to 50 K above the base temperature. After depositing butyl methyl sulfide at 5 K, the sample was heated to ≥30 K to ensure that all molecules had sufficient energy to reach their equilibrium adsorption sites. Alternatively, a given area could be "locally electrically annealed" by scanning over the molecules at 500 pA and 400 mV, which also equilibrated molecules to their preferred adsorption sites.

2.2. Theoretical Methods. Plane wave DFT calculations were performed with the Vienna ab initio simulation package (VASP) with the ultrasoft pseudopotentials available in this package.[33–35] The generalized gradient approximation (GGA) was employed with the Perdew−Wang 91 functional[36] and a plane wave cutoff energy of 286.7 eV. The geometries of the structures in these calculations were relaxed using a conjugate gradient algorithm until the forces on all unconstrained atoms were <0.03 eV/Å. All surface calculations used supercells defined using the DFT-optimized Au lattice constant, 4.182 Å. Au(111) was represented as a slab four layers thick with the bottom two layers constrained in its bulk positions. A vacuum spacing of 14 Å was used in the direction of the surface normal for all calculations. To avoid the interactions between adsorbates, all calculations were performed for a coverage corresponding to one molecule per supercell, that is, with an area of 121 Å^2/molecule using a (4 × 4) surface unit cell. All calculations used a 3 × 3 × 1 Monkhorst-Pack *k*-point mesh, which was sufficient to give well-converged results. The fcc termination is dominant in terms of area exposed in the 22 × √3 Au(111) reconstruction, and hence a fcc slab was used in all DFT calculations. When examining adsorption, molecules were placed on only one side of the slab. Dipole corrections were therefore applied in computing all of the energies reported below.[37,38] The nudged elastic band (NEB) method[39,40] was employed to investigate the energy barriers for both rotation and inversion of butyl methyl sulfide adsorbed on Au(111). The total number of intermediate images for each NEB calculation was five.

3. Results and Discussion

3.1. Asymmetric Dialkyl Sulfide Attachment: Chirality of the Adsorbed Species. When adsorbed on Au(111) at low coverages and annealed to ensure equilibration, the chirality of butyl methyl sulfide molecules can be inferred by their appearance in STM imaging. Figure 1a shows two mirror image pinwheels, which are the two surface-bound enantiomers of the otherwise achiral butyl methyl sulfide molecule. The pinwheel shape of these molecules is due to their rotation about the central Au−S bond[28,30–32] and their preferred orientation in one of the six near-equivalent directions on the Au(111) surface. (The rotational properties of these molecules are discussed in Section 3.2.) The asymmetric sulfide molecules attach to the Au surface through one of the two lone pairs on the sulfur and depending on which of these lone pairs bonds, this determines the surface-bound chirality of the molecule (Figure 1b).

DFT reveals that, consistent with STM images, adsorption on the Au surface gives the possibility for mirror symmetry of the adsorbed species. Figure 2a shows the calculated minimum energy adsorption site. Identification of this configuration was approached in a systemic way; the calculations were first performed with 11 initial configurations that varied the tilt angle of the molecule by increments of 5° relative to the surface normal. Using the most stable configuration obtained from these calculations, a new set of initial configurations were then

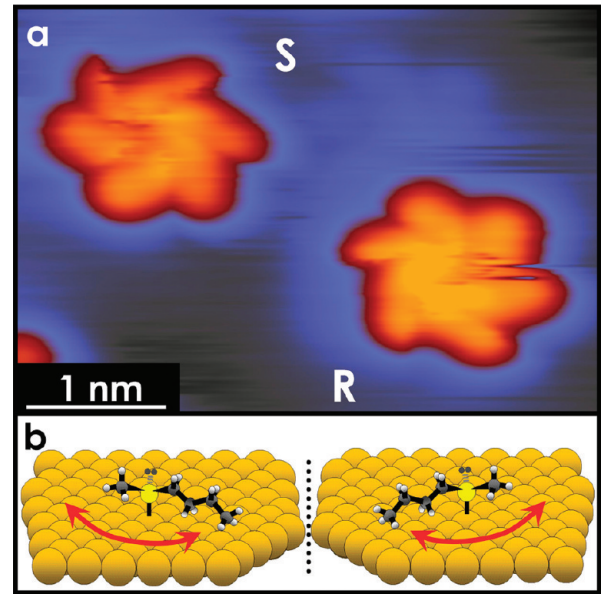

Figure 1. Two butyl methyl sulfide molecular rotors of opposite chirality. (a) Surface-induced chirality is apparent, as they are imaged as mirror-image pinwheels as they rotate about the central Au−S bond. Even though the temperature is low (5 K), the molecules rotate under perturbative tunneling conditions. (I = 400 pA, V = 300 mV, 5 K). (b) Schematic representation of the adsorption of the two enantiomers and their rotation about their central Au−S bond.

generated by rotating the molecule in the surface plane by increments of 10°. In total, therefore, 22 initial configurations were considered for the butyl methyl sulfide around the atop site of Au atom. Because previous calculations for the dimethyl sulfide adsorption on Au(111) demonstrated that the atop site is ∼0.3 eV more favorable than the fcc, hollow, hcp hollow, and bridge site,[32] these kinds of intensive calculations for the butyl methyl sulfide molecule were focused only on adsorption near the atop site of Au atom. Charge calculations by Bader analysis[41–43] show that upon this adsorption, a charge of −0.11e is transferred to the surface from the butyl methyl sulfide, indicating that in simple terms, adsorption to the surface occurs via binding of one of the lone pairs on the S atom. A charge density plot (Figure 2b) shows the nonbonding lone pair of the sulfur pointing off to the side of the molecule, which confirms that the molecule maintains its tetrahedral shape. With this geometry essentially unperturbed, attachment to the surface breaks the symmetry plane found in the gas-phase molecule and yields the chirality of the surface-bound molecules.

Using further DFT calculations, it was found that the barrier to inversion between the energetically equivalent enantiomers was 0.24 eV (Figure 3). This relatively high barrier is not surprising because the molecule must switch which lone pair binds to the surface to invert its chirality. This high barrier is also evidenced with STM experiments because the rotors were not observed to switch chirality under normal scanning conditions at either 5 or 78 K (see movie in Supporting Information). Only with high-energy electrons (>0.4 eV) supplied by the STM tip was it possible to overcome the high barrier to inversion and invert the chirality of the adsorbed molecules.[44,45]

3.2. Observed Rotational Properties of the Adsorbed Molecules. Both R and S enantiomers of butyl methyl sulfide rotate around their central Au−S bond axis. The six lobes of the chiral pinwheels shown in Figure 1 are due to the time-averaged superposition of six equivalent orientations of the molecule with respect to the underlying hexagonally packed surface. As shown in the DFT-minimized structure in Figure

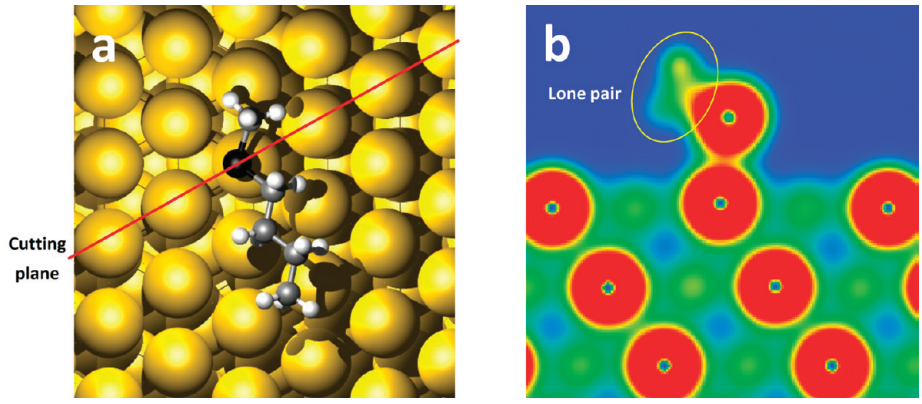

Figure 2. (a) Most stable DFT-optimized geometry of adsorbed butyl methyl sulfide on Au(111) and (b) its charge density contour map. The cutting plane for creating this map is also shown in part a.The position of the nonbonding lone pair is circled. The uppermost atom in red is the S atom, not to be confused with the other Au atoms (red) in the Au lattice.

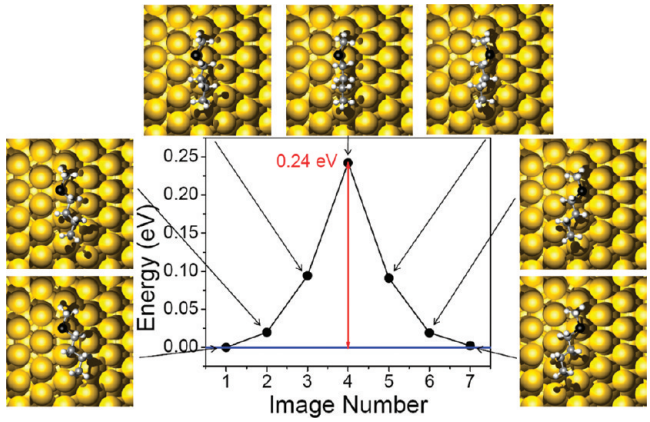

Figure 3. Nudged elastic band results for the inversion barrier between the energetically equivalent enantiomers. The inversion pathway for the adsorbed butyl methyl sulfide on Au(111) is exhibited along with each corresponding energy state. The barrier to this inversion is 0.24 eV.

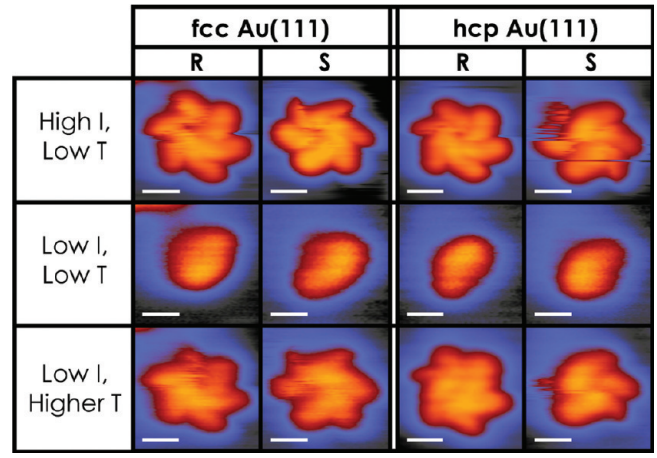

Figure 4. STM images of rotating and static R and S butyl methyl sulfide molecules in the fcc and hcp regions of the Au(111) surface. Top row: rotation caused by perturbative imaging conditions (higher tunneling currents and voltages). Middle row: static molecules under nonperturbative imaging conditions (low current and voltage). Bottom row: molecules rotating at nonperturbative imaging conditions due to a sample temperature increase from 5 to 10 K (tunneling conditions: top row: 300 pA, 300 mV, 5 K; middle row: 2 pA, 50 mV, 5 K; bottom row: 5 pA, 50 mV, 10 K). Scale bars = 0.5 nm.

2a, the butyl methyl sulfide molecules adsorb slightly off center of the traditional atop Au site. This off-center adsorption requires the S atom to precess as the molecule rotates to reproduce the six-fold symmetry seen in the STM images. The calculated maximum radius for the rotation of the S atom in the surface plane with respect to the center of a Au atom was 0.47 Å. This off-axis rotation has been characterized before[32] and explains the pinwheel appearance as opposed to a simpler hexagonal shape for the asymmetric sulfide molecule. The minimized structure calculated by DFT also allows for absolute chirality assignment of the surface-bound molecules based on the priorities around the central S atom of (1) the Au surface, (2) the butyl tail, (3) the methyl tail, and (4) the unbonded lone pair. This approach was used to assign the absolute chirality of each molecule in the STM image in Figure 1.

It is possible to induce the rotation of these molecules by either adjusting the tunneling conditions or heating the surface. As the 22 × $\sqrt{3}$ reconstruction of Au(111) leads to alternating regions of hcp and fcc atoms that can affect the preferential binding of adsorbates, molecules in both areas were studied independently. Figure 4 shows R and S molecules in both the hcp and fcc regions of the Au(111) surface. Molecular rotation can be induced even at 5 K by using perturbative imaging conditions (higher currents and voltages; top row of Figure 4), whereas lower currents and voltages allow for the molecules to be imaged as static, crescent-shaped molecules while they are not spinning (middle row of Figure 4). The crescent shape of the static molecule was predicted by the DFT calculations (Figure 2a), in which the tails were calculated to tilt toward the surface rather than perpendicular to the Au substrate. This led to their curved appearance with a protrusion nearer to one end of the molecule which was tentatively assigned as the S atom. At even slightly elevated temperatures the molecules have enough energy supplied by the temperature of the surface to rotate (bottom row of Figure 4). No noticeable differences were found between the rotational properties of rotors adsorbed on the fcc and hcp regions of the Au surface.

STM also affords the option to measure the rotational rates of these molecules. If the STM tip is placed to the side of one of the molecule's lobes, then all six positions of the butyl tail with respect to the underlying surface can be distinguished. In this measurement, the feedback loop (which is normally used to modulate the STM tip height to maintain a constant tunneling current) is turned off, and the tunneling current is monitored with respect to time (I vs t). Six current states can be measured for the six positions of the molecule with respect to the hexagonal Au surface (Figure 5). These states are a reflection of the proximity of an alkyl tail of the rotor molecule to the STM tip. (The closer the tail, the higher the tunneling current.)

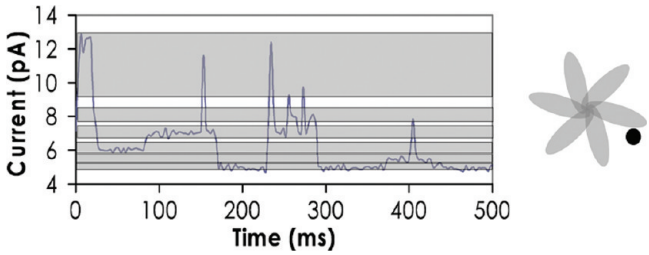

Figure 5. Current versus time (I vs t) curve shows rotational events as switches between six discrete current states. These states are due to six possible orientations of the molecule with respect to the STM tip (tunneling conditions: $I = 5$ pA, $V = 380$ mV, 5 K.)

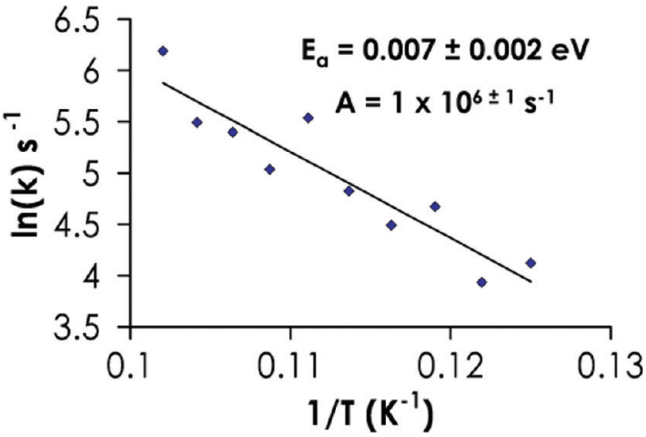

Figure 6. Arrhenius plot for a butyl methyl sulfide rotor (tunneling conditions: $I = 5$ pA, $V = 100$ mV).

By measuring how fast the alkyl tail changes position (and hence the rotational rate) as the temperature is increased, it is possible to further understand the rotational energetics (Figure 6). Arrhenius data is shown for a single butyl methyl sulfide molecule in the fcc region of the Au(111) surface. For simplicity only one region is shown; however, a plot for an hcp-adsorbed rotor can be found in the Supporting Information. (The fcc and hcp regions show similar rotational energetics within experimental uncertainties.) The activation energy (E_a) and the attempt frequency (A) calculated from these results are also displayed in Figure 6. All rates were calculated by measuring the number of switching events during the course of current versus time (I vs t) curves. The attempt frequency is noticeably low compared with the expected molecular event frequencies; however, this low attempt frequency has been previously observed for single molecule rotors. It has been postulated that the low A values arise because of multiple configurations of the alkyl tails in the ground state that lead to entropic effects in the transition state.[46–48]

To model the rotational barrier and further understand the shape of the rotating molecule, additional DFT calculations were performed. NEB calculations yielded a rotational energy barrier of 0.03 eV for a pathway involving the precession of the S atom around the top of an Au atom. (See Figure 7.) Other possible pathways were ruled out because they gave much higher rotational barriers. (See Supporting Information.)

The rotational energy barrier predicted by the DFT calculations is similar in magnitude to experimental observations, but the DFT barrier is ~4 times larger. Two caveats must be applied when quantitatively comparing these barriers. First, accurately resolving energy differences at the level of 0.01 eV is a challenging standard for any kind of quantum chemistry calculation, so it is perhaps unreasonable to expect that these

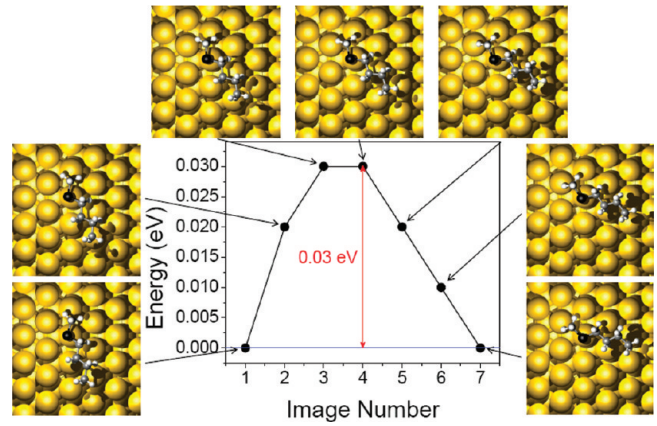

Figure 7. Nudged elastic band results for the rotational barrier of the S atom around the top of a Au atom. The rotation of this molecule by 60° was enough to cover the whole rotational path. The final state is equivalent to the initial state rotated by 60°. The rotational pathway for the adsorbed butyl methyl sulfide on Au(111) is exhibited along with each corresponding energy state. The barrier to this rotation is 0.03 eV.

calculations can make any statement more precise than confirming that the rotational energy barrier is small. Second, DFT calculations of this kind do not accurately account for dispersive interactions. For the dialkyl sulfide considered here, dispersive interactions between the molecule and the surface could vary slightly between the minimum energy state and the transition state for rotation, contributing to the net barrier for rotation. DFT calculations including semiempirical corrections for dispersion are now available,[35] but these methods are still subject to the challenge of precisely evaluating small energy differences discussed above.

4. Conclusions

Surface-bound butyl methyl sulfide molecules were studied using STM and DFT. This combination of experiment and theory allowed the equilibrium structure, rotational properties, and the barrier to rotation to be determined. Furthermore, high-resolution imaging revealed that the symmetry of the achiral molecule is broken upon adsorption to a surface. As the molecules bind to the surface primarily through just one of the lone pairs on the S, their tetrahedral geometry is preserved, and this leads to the appearance of two surface-bound enantiomers. DFT reveals that the barriers to inversion between the enantiomers are fairly high. This study indicates that the Au-sulfide bonds commonly used in organic, inorganic and materials chemistry can in fact have a chiral nature. Understanding the atomic-scale geometry and associated chirality of the Au−sulfide bond makes it easier to predict the surface properties of thioether linkers and highlights the possibility for diastereomeric effects when chiral sulfides are used.

Acknowledgment. All authors thank the NSF (grant no. 0717978) for financial support of this research and Prof. Andrew Gellman for helpful discussions. E.C.H.S. thanks Research Corporation and the Beckman Foundation for additional support. A.D.J. thanks NSF for a Graduate Research Fellowship. A.E.B. and H.L.T. thank the DOEd for GAANN fellowships.

Supporting Information Available: Butyl methyl sulfide purity verification with mass spectra, STM movie, Arrhenius plot for hcp-adsorbed butyl methyl sulfide, and DFT rotation pathway investigations. This material is available free of charge via the Internet at http://pubs.acs.org.

References and Notes

(1) Liu, W.; Howarth, M.; Greytak, A. B.; Zheng, Y.; Nocera, D. G.; Ting, A. Y.; Bawendi, M. G. *J. Am. Chem. Soc.* **2008**, *130*, 1274.

(2) Stuart, D. A.; Yuen, J. M.; Lyandres, N. S. O.; Yonzon, C. R.; Glucksberg, M. R.; Walsh, J. T.; Van Duyne, R. P. *Anal. Chem.* **2006**, *78*, 7211.

(3) Dameron, A. A.; Hampton, J. R.; Smith, R. K.; Mullen, T. J.; Gillmor, S. D.; Weiss, P. S. *Nano Lett.* **2005**, *5*, 1834.

(4) Love, J. C.; Estroff, L. A.; Kriebel, J. K.; Nuzzo, R. G.; Whitesides, G. M. *Chem. Rev.* **2005**, *105*, 1103.

(5) Donhauser, Z. J.; Mantooth, B. A.; Kelly, K. F.; Bumm, L. A.; Monnell, J. D.; Stapleton, J. J.; Price, D. W.; Rawlett, A. M.; Allara, D. L.; Tour, J. M.; Weiss, P. S. *Science* **2001**, *292*, 2303.

(6) Xia, Y. N.; Whitesides, G. M. *Angew. Chem., Int. Ed.* **1998**, *37*, 551.

(7) Li, X. M.; de Jong, M. R.; Inoue, K.; Shinkai, S.; Huskens, J.; Reinhoudt, D. N. *J. Mater. Chem.* **2001**, *11*, 1919.

(8) Maye, M. M.; Lim, I. I. S.; Luo, J.; Rab, Z.; Rabinovich, D.; Liu, T. B.; Zhong, C. J. *J. Am. Chem. Soc.* **2005**, *127*, 1519.

(9) Shelley, E. J.; Ryan, D.; Johnson, S. R.; Couillard, M.; Fitzmaurice, D.; Nellist, P. D.; Chen, Y.; Palmer, R. E.; Preece, J. A. *Langmuir* **2002**, *18*, 1791.

(10) Weidner, T.; Ballav, N.; Siemeling, U.; Troegel, D.; Walter, T.; Tacke, R.; Castner, D. G.; Zharnikov, M. *J. Phys. Chem. C* **2009**, *113*, 19609.

(11) Lavrich, D. J.; Wetterer, S. M.; Bernasek, S. L.; Scoles, G. *J. Phys. Chem. B* **1998**, *102*, 3456.

(12) Watson, D. J.; Jesudason, R.; Beaumont, S. K.; Kyriakou, G.; Burton, J. W.; Lambert, R. M. *J. Am. Chem. Soc.* **2009**, *131*, 14584.

(13) Illa, O.; Arshad, M.; Ros, A.; McGarrigle, E. M.; Aggarwal, V. K. *J. Am. Chem. Soc.* **2010**, *132*, 1828.

(14) Peterle, T.; Ringler, P.; Mayor, M. *Adv. Funct. Mater.* **2009**, *19*, 3497.

(15) Kautz, N. A.; Kandel, S. A. *J. Am. Chem. Soc.* **2008**, *130*, 6908.

(16) Maksymovych, P.; Yates, J. T. *J. Am. Chem. Soc.* **2008**, *130*, 7518.

(17) Nenchev, G.; Diaconescu, B.; Hagelberg, F.; Pohl, K. *Phys. Rev. B* **2009**, *80*, 081401.

(18) Stepanow, S.; Lin, N.; Payer, D.; Schlickum, U.; Klappenberger, F.; Zoppellaro, G.; Ruben, M.; Brune, H.; Barth, J. V.; Kern, K. *Angew. Chem., Int. Ed.* **2007**, *46*, 710.

(19) Makoudi, Y.; El Garah, M.; Palmino, F.; Duverger, E.; Arab, M.; Cherioux, F. *Surf. Sci.* **2008**, *602*, 2719.

(20) Weigelt, S.; Busse, C.; Petersen, L.; Rauls, E.; Hammer, B.; Gothelf, K. V.; Besenbacher, F.; Linderoth, T. R. *Nat. Mater.* **2006**, *5*, 112.

(21) Fasel, R.; Parschau, M.; Ernst, K. H. *Angew. Chem., Int. Ed.* **2003**, *42*, 5178.

(22) Bohringer, M.; Morgenstern, K.; Schneider, W. D.; Berndt, R.; Mauri, F.; De Vita, A.; Car, R. *Phys. Rev. Lett.* **1999**, *83*, 324.

(23) Rao, B. V.; Kwon, K. Y.; Zhang, J.; Liu, A. W.; Bartels, L. *Langmuir* **2004**, *20*, 4406.

(24) Troughton, E. B.; Bain, C. D.; Whitesides, G. M.; Nuzzo, R. G.; Allara, D. L.; Porter, M. D. *Langmuir* **1988**, *4*, 365.

(25) Jensen, S. C.; Baber, A. E.; Tierney, H. L.; Sykes, E. C. H. *ACS Nano* **2007**, *1*, 423.

(26) Jensen, S. C.; Baber, A. E.; Tierney, H. L.; Sykes, E. C. H. *ACS Nano* **2007**, *1*, 22.

(27) Noh, J.; Murase, T.; Nakajima, K.; Lee, H.; Hara, M. *J. Phys. Chem. B* **2000**, *104*, 7411.

(28) Baber, A. E.; Tierney, H. L.; Sykes, E. C. H. *ACS Nano* **2008**, *2*, 2385.

(29) Bellisario, D. O.; Baber, A. E.; Tierney, H. L.; Sykes, E. C. H. *J. Phys. Chem. C* **2009**, *113*, 5895.

(30) Tierney, H. L.; Baber, A. E.; Jewell, A. D.; Iski, E. V.; Boucher, M. B.; Sykes, E. C. H. *Chem.—Eur. J.* **2009**, *15*, 9678.

(31) Tierney, H. L.; Baber, A. E.; Sykes, E. C. H.; Akimov, A.; Kolomeisky, A. B. *J. Phys. Chem. C* **2009**, *113*, 10913.

(32) Tierney, H. L.; Calderon, C. E.; Baber, A. E.; Sykes, E. C. H.; Wang, F. J. *J. Phys. Chem. C* **2010**, *114*, 3152.

(33) Kresse, G.; Furthmuller, J. *Comput. Mater. Sci.* **1996**, *6*, 15.

(34) Kresse, G.; Hafner, J. *Phys. Rev. B* **1993**, *48*, 13115.

(35) Sholl, D. S.; Steckel, J. A. *Density Functional Theory: A Practical Introduction*; John Wiley & Sons: Hoboken, NJ, 2009.

(36) Perdew, J. P.; Chevary, J. A.; Vosko, S. H.; Jackson, K. A.; Pederson, M. R.; Singh, D. J.; Fiolhais, C. *Phys. Rev. B* **1992**, *46*, 6671.

(37) Bengtsson, L. *Phys. Rev. B* **1999**, *59*, 12301.

(38) Neugebauer, J.; Scheffler, M. *Phys. Rev. B* **1992**, *46*, 16067.

(39) Henkelman, G.; Jonsson, H. *J. Chem. Phys.* **2000**, *113*, 9978.

(40) Henkelman, G.; Uberuaga, B. P.; Jonsson, H. *J. Chem. Phys.* **2000**, *113*, 9901.

(41) Henkelman, G.; Arnaldsson, A.; Jonsson, H. *Comput. Mater. Sci.* **2006**, *36*, 354.

(42) Sanville, E.; Kenny, S. D.; Smith, R.; Henkelman, G. *J. Comput. Chem.* **2007**, *28*, 899.

(43) Tang, W.; Sanville, E.; Henkelman, G. *J. Phys.: Condens. Matter* **2009**, *21*, 084204.

(44) Simic-Milosevic, V.; Meyer, J.; Morgenstern, K. *Angew. Chem., Int. Ed.* **2009**, *48*, 4061.

(45) Parschau, M.; Passerone, D.; Rieder, K. H.; Hug, H. J.; Ernst, K. H. *Angew. Chem., Int. Ed.* **2009**, *48*, 4065.

(46) Briner, B. G.; Doering, M.; Rust, H. P.; Bradshaw, A. M. *Science* **1997**, *278*, 257.

(47) Chung, C. H.; Jung, W. J.; Lyo, I. W. *Phys. Rev. Lett.* **2006**, *97*, 116102.

(48) Jewell, A. D.; Tierney, H. L.; Baber, A. E.; Iski, E. V.; Laha, M. M.; Sykes, E. C. H. *J. Phys.: Condens. Matter*, in press.

JP1026702